

# Lasso-inspired peptides with distinct antibacterial mechanisms

Riadh Hammami · François Bédard · Ahmed Gomaa ·  
Muriel Subirade · Eric Biron · Ismail Fliss

Received: 25 June 2014 / Accepted: 17 November 2014 / Published online: 4 December 2014  
© Springer-Verlag Wien 2014

**Abstract** Microcin J25 (MccJ25) is an antibacterial peptide with a peculiar molecular structure consisting of 21 amino acids and a unique lasso topology that makes it highly stable. We synthesized various MccJ25-derived peptides that retained some of the inhibitory activity of the native molecule against *Salmonella enterica* and *Escherichia coli*. Of the tested peptides, **C1**, **7-21C** and **WK\_7-21** were the most inhibitory peptides (MIC = 1–250 µM), but all three were less potent than MccJ25. While MccJ25 was not active against Gram-positive bacteria, the three derived peptides were slightly inhibitory to Gram-positive bacteria (MIC ≥ 250 µM). At 5 µM, **C1**, **7-21C** and **WK\_7-21** reduced *E. coli* RNA polymerase activity by respectively, 23.4, 37.4 and 65.0 %. The MccJ25 and its derived peptides all appeared to affect the respiratory apparatus of *S. enterica*. Based on circular dichroism and FTIR spectroscopy, the

peptides also interact with bacterial membrane phospholipids. These results suggest the possibility of producing potent MccJ25-derived peptides lacking the lasso structure.

**Keywords** Antimicrobial peptides · Microcin J25 · Solid phase peptide synthesis · Antibacterial activity · Mode of action

## Introduction

Microcin J25 (MccJ25) is a 21-residue ribosomally synthesized bactericidal peptide with an unusual lariat protoknot structure (Bayro et al. 2003; Wilson et al. 2003; Rosengren et al. 2003). It is produced by *Escherichia coli* strains that harbor the plasmid-borne *mcjABCD* biosynthetic gene cluster (Solbiati et al. 1996). Mature MccJ25 is produced from a 58-amino-acid precursor called McjA following cleavage by ATP-dependent cysteine protease McjB and intramolecular cyclization catalyzed by amidotransferase McjC (Yan et al. 2012; Clarke and Campopiano 2007). It is then transported and exported into the extracellular milieu by ATP-binding cassette (ABC) transporter McjD encoded by the *mcjD* gene (Choudhury et al. 2014).

MccJ25 exhibits bactericidal activity toward several Gram-negative food-borne pathogens, including *Salmonella*, *Shigella* and *E. coli* (Sable et al. 2000; Vincent et al. 2004). The particular lasso topology of MccJ25 makes the peptide highly resistant to denaturation by high temperatures or proteolysis. These are attractive properties to both the food and pharmaceutical industries. MccJ25 structure consists of an 8-residue cycle (lariat ring) formed by a lactam (isopeptide) bond between the N-terminal amide and the carboxyl group of a glutamic acid side chain, which is followed by a 13-residue tail that loops back to thread

**Electronic supplementary material** The online version of this article (doi:10.1007/s00726-014-1877-x) contains supplementary material, which is available to authorized users.

R. Hammami (✉) · A. Gomaa · M. Subirade · I. Fliss (✉)  
STELA Dairy Research Centre, Institute of Nutrition  
and Functional Foods, Université Laval, Québec,  
QC G1V 0A6, Canada  
e-mail: riadh.hammami@fsaa.ulaval.ca

I. Fliss  
e-mail: Ismail.fliss@ulaval.ca

F. Bédard · E. Biron  
Faculty of Pharmacy, Université Laval and Laboratory  
of Medicinal Chemistry, CHU de Québec Research Centre,  
Québec, QC G1V 4G2, Canada

## Present Address:

A. Gomaa  
Food Technology and Nutrition Research Division, Food Science  
and Nutrition Department, National Research Center,  
Cairo, Egypt

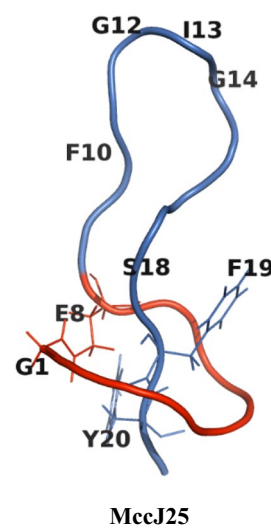
through the ring (Fig. 1). The C-terminal tail (residues 9–21) of the peptide is tightly (irreversibly for all practical purposes) trapped in the lariat ring due to the presence of two aromatic side chains at positions 19 and 20. The overall folding includes a  $\beta$ -hairpin involving two  $\beta$ -strands (10–11 and 15–16) connected by a  $\beta$ -turn pattern (11–14). MccJ25 bears only two charged groups: histidine at position 5 (positive charge) and the C-terminal carboxyl group of Gly21 (negative charge). These are reportedly important for the activity of the peptide (Bellomio et al. 2003).

Uptake of MccJ25 by target bacterial cells involves the iron transporter FhuA located in the outer membrane (Salomón and Farías 1993), the energy transduction complex TonB-ExbB-ExbD (Braun 1995), and the inner membrane protein SbmA (Salomón and Farías 1995). RNA polymerase appears to be the principal intracellular target of MccJ25 (Delgado et al. 2001; Yuzenkova et al. 2002), which binds within and obstructs the secondary channel, thus interfering with diffusion of nucleoside triphosphate substrate to the enzyme catalytic site (Mukhopadhyay et al. 2004). MccJ25 also possesses multiple independent mechanisms of action that appear to affect different intracellular targets including the respiratory chain (Bellomio et al. 2007; Niklison Chirou et al. 2008).

A cleaved MccJ25 obtained by thermolysin cleavage in the  $\beta$ -hairpin loop retained bioactivity against *Salmonella enterica* serovar Newport but not against *E. coli* MC4100, suggesting that the mechanism of action might be different depending on the target strain (Blond et al. 2002). The

$\beta$ -hairpin loop region appears important for peptide uptake by FhuA, but not for binding to RNAP (Bellomio et al. 2004; Semenova et al. 2005; Destoumieux-Garzón et al. 2005). In contrast, the C-terminal region appears to be essential for RNAP inhibition. Amidation of the C-terminal glycine inhibits MccJ25 binding to RNAP but not its uptake by cells or its effect on respiration (Vincent et al. 2005). The histidine residue of the lariat ring (His5) has been shown important for recognition of the peptide by the inner membrane receptor SbmA (de Cristóbal et al. 2006). In addition, mutations in largest subunit of RNAP leading resistance to MccJ25 have provided a more detailed information on MccJ25 binding to RNAP secondary channel (Yuzenkova et al. 2002). More recently, structure–activity relationships were examined using multiple MccJ25 variants constructed by site-directed mutagenesis and screened for antibacterial activity and ability to inhibit RNAP (Pan and Link 2011; Pavlova et al. 2008; Pan et al. 2011; Ducasse et al. 2012). These studies revealed that the inhibitory activity of MccJ25 tolerates a number of residue substitutions.

Recent attempts to produce the lasso structure of MccJ25 through chemical synthesis (yielding a loop–tail rather than a lasso topology) have not yielded successful microbial inhibitors (Ferguson et al. 2010). Nevertheless, two of six synthetic peptides derived from MccJ25 without lasso folding were found to be bactericidal (Soudy et al. 2012). We hypothesized that lasso formation is important but not a prerequisite for the activity of MccJ25 and that it may be possible to obtain derivatives that are active without



Peptide	Sequence	Bonds	Mass MH <sup>+</sup> (mono)	Net charge
MccJ25	GGAGHVPEYFVGIGTPISFYG	1-8	2 107.04	0
1-8L	GGAGHVPE-----	-	723.34	-1
1-10C	GGAGHVPEYF-----	1-8	1 031.47	0
NC1	GGAGHVPCYF-GKG---CFYG	8-18	1 717.74	+1
NC2	GGAGHVPCYF-KKK---CFYG	8-18	1 859.89	+3
NC3	GGAGHVPCYF-WKW---CFYG	8-18	1 975.85	+1
9-21L	-----YFVGIGTPISFYG-NH <sub>2</sub>	-	1 420.71	0
9-21C	-----H <sub>2</sub> N-CFVGIGTPICFYG-NH <sub>2</sub>	9-18	1 373.65	0
8-21C	-----CYFVGIGTPICFYG	8-18	1 537.70	0
7-21C	-----KCYFVGIGTPICFYG	8-18	1 665.79	+1
WK_7-21	GWKGKWKCYFVGIGTPICFYG	8-18	2 408.19	+3
C1	CGAGHVPCYFVGIGTPISFYG	1-8	2 142.99	0
C2	CGAGHVPEYFVGIGTPICFYG	1-18	2 185.00	-1
C3	GGAGHVPCYFVGIGTPICFYG	8-18	2 112.98	0

**Fig. 1** Amino acid sequence, molecular weight and net charge of MccJ25 and derived-peptides thereof. Amide and disulfide bonds are colored in blue and yellow respectively (color figure online)

the lasso structure. In this study, we report synthetic peptides based on the MccJ25 sequence but devoid of lasso folding yet retaining activity against bacteria (*S. enterica* and *E. coli*) and specific intracellular targets (RNA polymerase and the respiration chain). The antimicrobial activity, mode of action, toxicity and conformation of the synthesized peptides were evaluated.

## Materials and methods

### Materials

All reagents and solvents were purchased from commercial suppliers and used without additional purification. Amino acid derivatives and coupling reagents 2-(6-chloro-1H-benzotriazole-1-yl)-1,1,3,3-tetramethylammonium hexafluorophosphate (HCTU) and benzotriazol-1-yl-oxy-tris(pyrrilidino)phosphonium hexafluorophosphate (PyBOP) were purchased from Matrix Innovation Inc. (Quebec, QC, Canada). Rink Amide AM resin (0.65 mmol/g) and 2'-chlorotriyl chloride resin (2-Cl-Trt) (1.6 mmol/g) were purchased from ChemImpex (Wood Dale, IL, USA). Reactions on solid support were performed in polypropylene-fritted syringes from Roland Vetter Labordedarf OHG (Ammerbuch, Germany).

### Bacteria, media and growth conditions

The reference strains used in this study (Table 1) were maintained in 20 % glycerol at  $-80^{\circ}\text{C}$ . All were grown in tryptic soy broth (TSB; Difco Laboratories, Sparks, MD, USA) supplemented with 0.6 % (w/v) yeast extract and were incubated aerobically at  $30^{\circ}\text{C}$ . Before the experiments, strains were sub-cultured at least three times in their respective media at 24 h intervals. Minimal medium M63 supplemented with glucose (0.2 %, w/v) and thiamine (0.01 %, w/v) was used for MccJ25 production.

### Microcin J25 production and purification

A clone of *E. coli* MC4100 harboring the plasmid pTUC202 (courtesy of Dr. Sophie Sablé, Université La Rochelle, France) was used for production and purification of MccJ25 as described previously (Sable et al. 2000).

### Peptide synthesis and purification

#### General procedure

Peptides were synthesized by standard Fmoc solid-phase synthesis using 2-Cl-Trt resin (Fields and Noble 1990). Briefly, the Fmoc protecting group was removed from

**Table 1** Minimal inhibitory concentrations of MccJ25 and its derivatives for bacteria

Bacterial strain	Minimal inhibitory concentration ( $\mu\text{M}$ )							
	MccJ25 <sup>a</sup>	NC2	NC3	C1	C3	8-21C	7-21C	WK_7_21
<i>Salmonella enterica</i> subsp. <i>enterica</i> ATCC 14028	6.5	—	—	125–250	—	—	—	—
<i>Salmonella enterica</i> subsp. <i>enterica</i> ATCC 8387	0.1	—	31.3	1.0	15.6–31.3	1.0	7.8–15.6	7.8
<i>Salmonella enterica</i> subsp. <i>enterica</i> ATCC 29628	6.5	250	—	—	—	—	—	—
<i>Salmonella enterica</i> subsp. <i>enterica</i> ATCC 8400	0.8	—	—	62.5–125	—	—	125–250	62.5
<i>Salmonella enterica</i> subsp. <i>enterica</i> ATCC 9607	1.6	—	—	250	—	—	—	—
<i>Salmonella enterica</i> subsp. <i>enterica</i> ATCC 9700	0.4	—	—	250	—	—	—	—
<i>Escherichia coli</i> ATCC 11229	0.2	—	—	62.5	—	125–250	—	250
<i>Escherichia coli</i> ATCC 25922	3.3	—	—	250.0	—	—	250	—
<i>Escherichia coli</i> ATCC 15144	—	—	—	—	—	—	—	—
<i>Escherichia coli</i> O157:H7 ATCC 35150	—	—	—	—	—	—	—	—
<i>Escherichia coli</i> MC4100 ATCC 35695	6.5	—	—	31.3–62.5	—	—	125	—
<i>Escherichia coli</i> DH5a	6.5	—	—	—	—	—	—	—
<i>Escherichia coli</i> LR 05	—	—	—	>250	—	—	>250	>250
<i>Listeria ivanovii</i> HPB28	—	—	—	>250	—	—	>250	250
<i>Staphylococcus aureus</i> ATCC 6538	—	—	—	>250	—	—	ND	>250
<i>Enterococcus faecalis</i> ATCC 27275	—	—	—	>250	—	—	ND	>250

>250 = Partial inhibition at 250  $\mu\text{M}$  and MIC value is higher than 250  $\mu\text{M}$ . Peptides 1-8L, 1-10C, NC1, 9-21L, 9-21C and C2 were not inhibitory at concentrations up to 250  $\mu\text{M}$

“—” No activity detected at concentrations up to 250  $\mu\text{M}$ , ND not determined

<sup>a</sup> Produced by bacteria

the resin by two 10 min treatments with 20 % piperidine in DMF (v/v) and amino acid coupling was performed with Fmoc-Xaa-OH (3 eq.), HCTU (3 eq.) and *N*-methylmorpholine (12 eq.) in DMF (2 × 30 min). The synthesized peptide was released by treating the resin with 20 % HFIP in DCM for 30 min (Bollhagen et al. 1994). The solvent was removed under reduced pressure and side chain de-protection was achieved by treating with TFA/TIPS/H<sub>2</sub>O (95:2.5:2.5) for 3 h. The resulting peptides were precipitated with cold ether and purified by RP-HPLC with a Shimadzu Prominence instrument (Columbia, MD, USA) on a Vydac 218MS column (22.0 × 250 mm, 300 Å, 10 µm, C18) using 0.1 % TFA/H<sub>2</sub>O (solvent A) and 0.1 % TFA/CH<sub>3</sub>CN (solvent B) with a linear gradient of 10–100 % solvent B for 20 min at 10 ml min<sup>-1</sup> and UV detection at 220 and 254 nm. After freeze-drying, the purified peptides were characterized by matrix-assisted laser desorption ionization time-of-flight mass spectrometry (MALDI-TOF) on an AB SCIEX 4800 Plus MALDI-TOF/TOF instrument using alpha-cyano-4-hydroxycinnamic acid as matrix.

#### Cyclization on resin

Tail-to-side-chain cyclization was performed on peptides containing a Glu(OAll) residue. The resin-bound fully protected peptide was treated with Pd(PPh<sub>3</sub>)<sub>4</sub> (0.4 eq.) and PhSiH<sub>3</sub> (12 eq.) in DCM (2 × 40 min) to remove the allyl group, followed by washing with DCM (5×), 0.5 % (v/v) DIPEA/DMF (2×), 5 % (v/v) diethyl dithiocarbamate/DMF (2×) and DMF (5×) (Patel et al. 1999). After Fmoc group removal as described above, peptide cyclization was performed on solid support in the presence of PyBOP (3 eq.) and DIPEA (6 eq.) in DMF for 3 h. Cyclization was monitored using the chloranil test and after reaction completion, the resin was washed with DMF (5×) and DCM (5×). The cyclic peptides were cleaved, purified and characterized as described above.

#### Oxidative folding and disulfide bond formation

Fully de-protected crude peptide was dissolved in a mixture of 80 % DMSO/H<sub>2</sub>O and the solution was adjusted to pH 6 with AcOH (Tam et al. 1991). The mixture was stirred for 3–5 days and disulfide bond formation was monitored by LC-MS. After complete disulfide bridge formation, the solvent was removed by freeze-drying. The oxidized peptide was purified and characterized as described above.

#### Minimal inhibitory concentration (MIC) evaluation

The minimal inhibitory concentrations (MIC) were determined using polystyrene micro-assay plates (96-well

Microtest, Becton–Dickinson Labware, Sparks, MD, USA) as described by Hammami et al. (2009). Briefly, micro-plates loaded with twofold serial dilutions of each peptide (starting at 250 µM) in TSB were seeded with log-phase culture of target strain diluted in TSB to 0.5–1.0 × 10<sup>6</sup> cfu ml<sup>-1</sup> (approximately 1 × 10<sup>4</sup> cfu per well). Micro-plates were then incubated at 37 °C for 24 h and absorbance at 595 nm was measured hourly using an Infinite® F200 PRO photometer (Tecan US inc., Durham, NC, USA). MIC values were expressed in µM and correspond to the lowest concentration that inhibited the growth of target organism after 16–20 h. The MIC values are reported as means of two independent experiments in duplicate.

#### RNAP inhibition assay

Inhibition of *E. coli* RNAP in vitro by MccJ25 and its derivatives were assayed by amplifying transcripts of the Kool NC-45 universal RNA polymerase template (Epicentre, Madison, WI, USA). The assay was performed according to the manufacturer's protocol and amplification was quantified using qRT-PCR. Rifampicin (200 nM) was used to obtain total inhibition.

#### Oxygen consumption

An overnight culture of *S. enterica* (OD<sub>595</sub> = 0.4–0.5) in TSYB was diluted in medium to an OD<sub>595</sub> of 0.2 and incubated for 30 min at 37 °C with MccJ25 or derivative. The average rate of respiration over the subsequent 5 min was measured using a Gilson Clark-type polarographic electrode oxygraph. A control sample in the absence of peptide was also measured.

#### Hemolysis assays

Peptide hemolytic activity was measured as hemoglobin release by lysis of horse red blood cells. Fresh erythrocytes were washed three times with sodium phosphate buffer saline (PBS) (100 mM, pH 7.4) and diluted to 5 % (v/v) in the buffer. Erythrocyte suspension (100 µl) was mixed with peptide at different concentrations (100 µl) in PBS, held at 37 °C for 1 h and then centrifuged for 5 min. Positive and negative controls were run using 100 µl of 1 % Triton X-100 solution or PBS. Intact erythrocytes were pelleted by centrifugation at 1,000×g for 5 min at 4 °C and hemoglobin release was monitored by measuring absorbance at 450 nm. All samples were prepared in triplicate and run three separate times to ensure reproducibility. Percent hemolysis was defined as follows: [(sample absorbance × phosphate buffer absorbance)/Triton X-100 absorbance] × 100.

## Preparation of liposomes

Lipids dissolved in methanol were dried under nitrogen stream and re-suspended in 100 mM phosphate buffer, either in water at pH 7.4 or in deuterium oxide at pD 6.0. To obtain small unilamellar vesicles, the formed multilamellar liposomes were subjected to sonication using a probe sonicator (6 W, 60 Sonic Dismembrator, Fisher Scientific, USA) at intervals of 30 s for 20 min at 5 °C followed by centrifugation at 12,000×g.

## Circular dichroism (CD) measurements

CD measurement of each peptide (2 mg ml<sup>-1</sup>) in 100 mM phosphate buffer at pH 7.2 was performed with a Jasco J-815 spectrometer (Aviv Instruments, Lakewood, NJ, USA). The spectra were recorded at 25 °C in the 195–250 nm wavelength range at 0.1 nm intervals in a cuvette with a 0.5 mm path length. For each spectrum, five scans were averaged and smoothed by the J720/98 system program (Version 120C). CD data were expressed as mean residue ellipticity [Θ] given in deg cm<sup>2</sup> dmol<sup>-1</sup>, plotted against wavelength (nm) and analyzed using the CONTIN algorithm included in the CDPPro analysis software.

## FTIR analysis

Infrared spectra at a resolution of 2 cm<sup>-1</sup> were recorded with a Magna Nicolet 560 spectrometer (Madison, WI, USA) equipped with an MCT (mercury–cadmium–telluride) detector and continuously purged with dried air. Pure phospholipids in addition to the mixtures (10:1 w/w) of each phospholipid with individual tested peptides were prepared in D<sub>2</sub>O and mixed for 1 h prior to the analyses. The samples were placed between CaF<sub>2</sub> windows separated by spacer 23 μm thick. The samples were first cooled to 5 °C and spectra were collected over the range of 5–80 °C in 5 °C increments except for the 15–45 °C range in which data were collected at each 2 °C increment to monitor the chain-melting phase transition in detail. Each spectrum represented an average of 128 scans apodized with a Happ-Ganzel function. The wavenumber of the symmetric C–H stretching mode [ $\nu_s(\text{CH}_2)$ ] for the acyl chain methylene groups of the lipids was determined after subtracting a linear baseline from the 3,050–2,750 cm<sup>-1</sup> region.

## Statistical analysis

Data are presented as mean ± standard deviation of three independent experiments. Data were subjected to ANOVA using the GLM procedure of SAS (SAS Institute, Inc., Cary, NC, USA). A multiple comparison test (LSD) was used to reveal significant differences between the treatment means ( $P \leq 0.05$ ).

## Results

### Peptide design

In this study, we designed in silico and then synthesized various peptides based on the primary structure of MccJ25 (Fig. 1). The peptide code is based on MccJ25 numbering. We evaluated the antibacterial activity of shortened N-terminal and C-terminal sequences since cleaved MccJ25 has been shown previously to be antibacterial (Blond et al. 2002). The lariat ring was synthesized in linear **1-8L** and cyclized **1-10C** forms. The tail (C-terminal) portion was synthesized as linear peptide **9-21L**. A disulfide bond was introduced between C9 and C18 to form the head-to-tail circular peptide **9-21C**. Peptides **8-21C**, **7-21C** and **WK\_7-21** are designed from a tail that was scaffold-stabilized using a disulfide bond between cysteine residues substituted at positions 8 and 18. While a single lysine residue was inserted at the N-terminus of **7-21C**, peptide **WK\_7-21** was obtained by substituting the N-terminal portion of MccJ25 with multiple hydrophobic (tryptophan) and basic (lysine) and residues (NH<sub>2</sub>-GWKGKWK) to increase solubility and possibly induce β-hairpin structure. In addition, peptides **C1**, **C2** and **C3** containing a single disulfide bond (1–8, 1–18 or 8–18) were designed to retain the core structure of the native MccJ25 peptide regardless of the lariat protoknot structure. **NC1**, **NC2** and **NC3** were synthesized with deletions in the loop and tail regions of the lasso.

### Evaluation of antimicrobial activity and toxicity

Table 1 summarizes the minimum inhibitory activities (MICs) of the synthesized peptides in comparison to bacteria produced microcin. Synthetic peptides that had no activity on the strains tested at and below 250 μM are not listed in Table 1. The MccJ25 peptide was active at micromolar and nanomolar concentrations (0.1–6.5) against Gram-negative bacteria, with *S. enterica* ATCC 8387 being the most sensitive strain (MIC = 0.1 μM). While peptide **C2** was not inhibitory, **C1** inhibited several strains of *S. enterica* and *E. coli*. Against *S. enterica* ATCC 8387, the MICs of peptides **C1**, **C3**, **8-21C**, **7-21C** and **WK\_7-21** were respectively, 1.0, 15.6–31.3, 1.0, 7.8–15.6 and 7.8 μM. Inhibition of *S. enterica* ATCC 8387 by MccJ25 and its derived peptides at 0.5 and 7.8 μM is summarized in Fig. 2. At 0.5 μM, the derived peptides were moderately inhibitory (25–50 %). Similarly to MccJ25, inhibition by **C1**, **8-21C** and **WK\_7-21** was total at 7.8 μM (above the MIC). Although MccJ25 was not active against Gram-positive bacteria, peptides **C1**, **7-21C** and **WK\_7-21** were weakly inhibitory to *Listeria ivanovii* HPB28, *Staphylococcus aureus* ATCC 6538 and *Enterococcus faecalis* ATCC 27275 (MIC ≥ 250 μM).

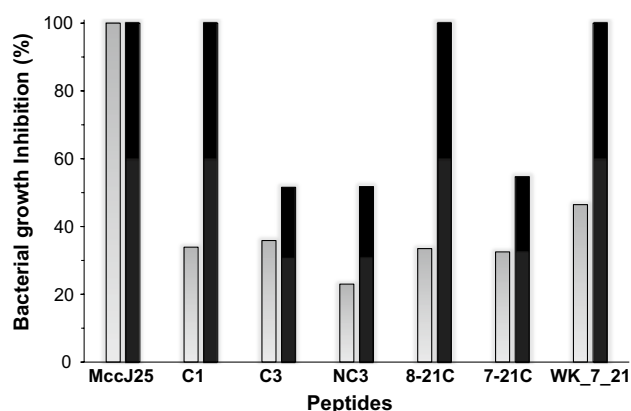


**Fig. 2** Inhibition of growth of *Salmonella enterica* subsp. *enterica* ATCC 8387 by MccJ25 and its derived peptides (C1, C3, NC3, 8-21C, 7-21C and WK\_7-21) at 0.5 μM (gray) and 7.8 μM (black). Data are means of triplicate measurements

Of the synthetic MccJ25-derived peptides described previously, two in particular, namely GGACHVPEYFV GIGTPISFC (“peptide 1” bonded 1–8, 4–20) and CGAGF HVPCYFVGRGTPISFYG (“peptide 6” bonded 1–9), were inhibitory to *Salmonella newport* at MICs of 25 and 30 μM, respectively (Soudy et al. 2012). While peptide **C1** of this study was designed with the replacement of the amide bond between G1 and E8 by a disulfide bond, peptide **6** contained besides a phenylalanine insertion at position 5 and an arginine substitution for isoleucine at position 13. Although these mutations increased the solubility of peptide **6**, they decreased its inhibitory action. While peptide **C1** was inhibitory to Gram-negative pathogens, peptide **6** was 60 times less potent than MccJ25 against *S. enterica* Newport and **C1** against *S. enterica* ATCC 8387 were 10 times less potent than MccJ25. Further, **C1** showed a weak activity against Gram-positive bacteria (MIC > 250 μM). Soudy et al. (2012) also reported absence of activity for a peptide **6** variant with an 8-residue lariat ring. Based on our results, the glycine substitution by phenylalanine at position 4 could explain the decrease of activity observed for peptide **6** and its variant compared to **C1**. The arginine substitution at position 13 has been reported previously to increase the antimicrobial activity of MccJ25 (Pavlova et al. 2008). In this study, different synthetic derivatives of MccJ25 containing substitutions and/or truncations exhibited antibacterial activity against Gram-negative bacteria. Although the reduced activity of these designed synthetic derivatives compared to the native MccJ25, the lasso fold does not seem to be a prerequisite for the antimicrobial activity.

The hemolytic activity of MccJ25, **C1**, **7-21C** and **WK\_7-21** towards horse erythrocytes is shown in Fig. 3. All four peptides were weakly hemolytic (<6 %) up to the

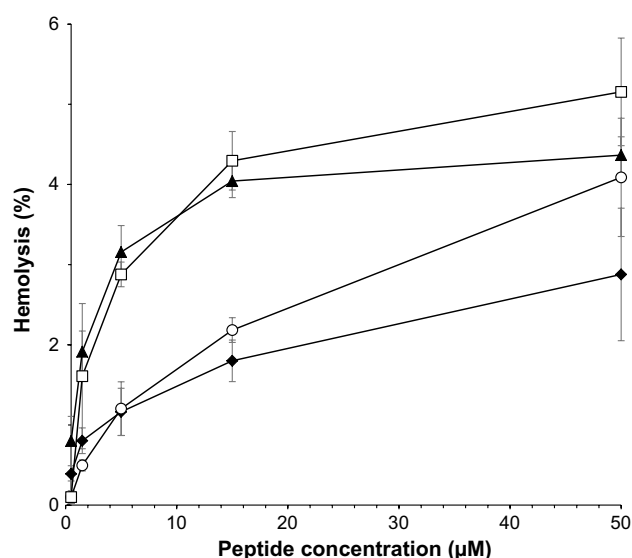


**Fig. 3** Hemolysis of horse red blood cells by MccJ25 (triangle), C1 (circle), 7-21C (diamond) and WK-7-21 (square). A 1 % (w/v) solution of Triton X-100 was the positive control. The values are mean ± SD of triplicate analyses

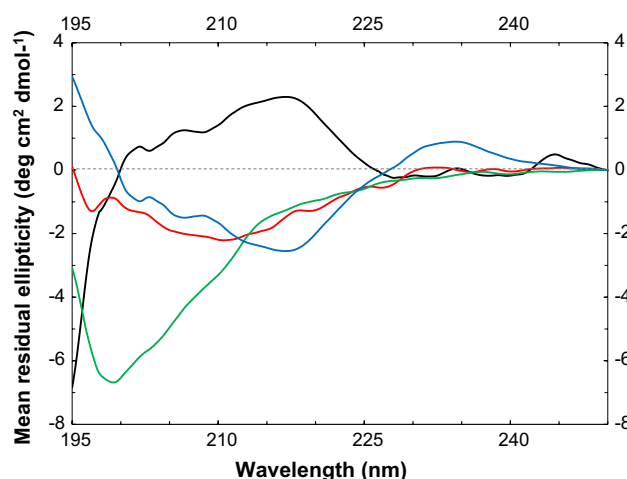


**Fig. 4** Circular dichroism spectra for MccJ25 (black), C1 (blue), 7-21C (green) and WK\_7-21 (red) (color figure online)

highest tested concentration (50 μM), which is consistent with the low toxicity reported in the literature (Lopez et al. 2007; Soudy et al. 2012). Overall, hemolysis did not differ significantly at 50 μM ( $P > 0.05$ ). MccJ25 and its derivatives are thus good candidates for therapeutic application, although it is to point that concentration range for hemolysis and antibacterial activity is about the same for the synthetic peptides (maximum 5 times higher), while the concentration inducing hemolysis (depending on the target bacteria) is 10–100 times higher than that for antibacterial activity in the case of MccJ25.

## Structural characterization of peptides using circular dichroism (CD)

CD spectroscopy in the far-UV region (195–250 nm) is frequently used to characterize molecular secondary structure. The peaks of the CD spectrum of MccJ25 (Fig. 4) are due to the lasso structure and the transition modes of phenylalanine and tyrosine residues near the loop. The minimal ellipticity at 195 nm is assigned to  $\beta$ -strands forming the  $\beta$ -hairpin structure (Liu et al. 2008; Soudy et al. 2012). In addition, a positive peak at 218 nm and two shoulders at 206 and 202 nm are attributable to side chain transitions of Tyr and Phe, respectively (Sreerama and Woody 2004). The broad spectrum with a minimum ellipticity at 200 nm (e.g. peptide **7-21C**) typifies the random coil structure (Kelly and Price 2000). Furthermore, peptides **C1** and **WK\_7-21** showed broadened spectra suggesting the existence of a folded secondary structure differing from that of MccJ25 (Fig. 4). The MccJ25 spectrum is largely in agreement with a previous report of a trough at 200 nm and a peak at 215 nm with a shoulder at 210 nm (Soudy et al. 2012), although the CD measurements were made under conditions (e.g., protein concentration, polarity of the buffer) differing from those used in the present study.

## Mode of action

### RNAP inhibition

The inhibition of RNAP by MccJ25, **9-21L**, **C1**, **C3**, **7-21C** and **WK\_7-21** was examined in vitro (Fig. 5). Rifampicin, an antibiotic that targets bacterial RNAP was used as a control. MccJ25 was the best inhibitor, reducing *E. coli* RNAP activity by 86.3 and 97.9 %, respectively at 5 and 50  $\mu$ M. Peptides **C1**, **7-21C** or **WK\_7-21** at a concentration of 5  $\mu$ M reduced activity by 23.4, 37.4 and 65.0 %, respectively. Linear peptide **9-21L**, which is inactive, was not inhibitory. At 50  $\mu$ M, reductions by MccJ25, **C1** and **WK\_7-21** were 97.9, 95.7 and 94.7 %, respectively, while **C3** (not inhibitory at 5  $\mu$ M) reduced RNAP activity by 70.6 %. These results suggest that the MccJ25-derived peptides could inhibit *E. coli* by interacting with RNAP and thereby interfering with transcription.

### Inhibition of cell respiration

The ability of MccJ25, **C1**, **C3**, **7-21C** and **WK\_7-21** to inhibit respiration of *S. enterica* ATTC 8387 is shown in terms of MIC in Fig. 6. The decrease in oxygen consumption by *S. enterica* after incubation with MccJ25 was 57.2 %. **WK\_7-21** was the strongest inhibitor among the synthetic peptides, decreasing oxygen consumption by 36.9 %, followed by **C1** and **7-21C** at 32.1 and 24.2 % and

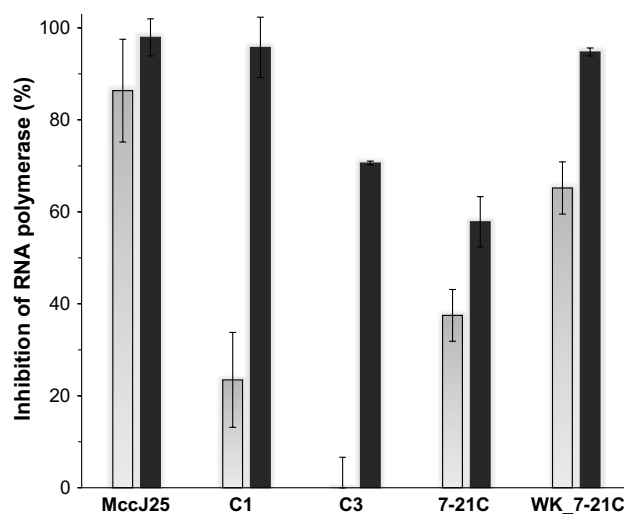


**Fig. 5** Inhibition of *E. coli* RNA polymerase in vitro by MccJ25 and peptides **C1**, **C3**, **7-21C** and **WK\_7-21** at 5  $\mu$ M (gray) and 50  $\mu$ M (black). Rifampicin (200 nM) was the positive control. The values are mean  $\pm$  SD of triplicate analyses

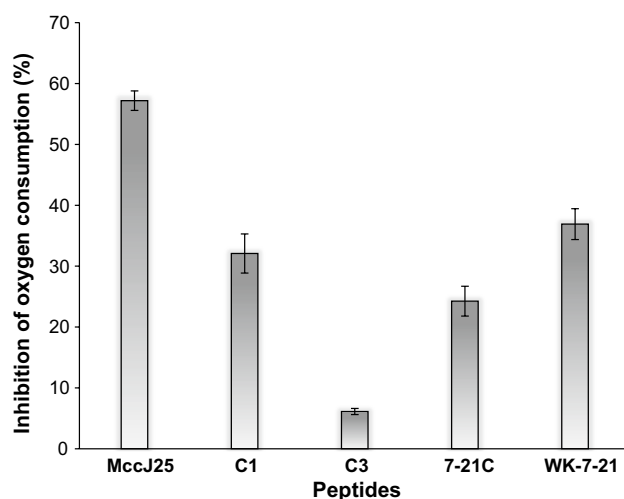


**Fig. 6** Inhibition of oxygen consumption by MccJ25 and peptides **C1**, **C3**, **7-21C** and **WK\_7-21** at their respective MICs. The values are mean  $\pm$  SD of triplicate analyses

finally **C3** at only 6.1 %. The antibacterial action of this peptide is therefore likely due to some other mechanism. Inhibition of respiration by peptides **WK\_7-21**, **C1** and **7-21C** suggests that they share at least one mechanism of action with MccJ25.

### Interaction of peptides with membrane lipids using circular dichroism (CD)

To investigate the conformational behavior of MccJ25 and its synthetic derivatives **C1**, **7-21C** and **WK\_7-21** both

outside and within membranes, studies of the average secondary structure adopted by these peptides in the absence or presence of phospholipid vesicles were conducted using CD spectroscopy. Eukaryotic cell membranes are composed primarily of zwitterionic lipids, in particular phosphatidylcholine (PC), while the outer envelope of bacterial cells contains a variable mixture of anionic (phosphatidylglycerol, PG) and zwitterionic (phosphatidylethanolamine, PE) lipids. We used palmitoyl-oleoyl (PO) PG anionic vesicles and either POPC or POPE zwitterionic vesicles. Predicted secondary structures based on data deconvolution are presented in supplementary Table S1. MccJ25 alone adopted a secondary structure composed mainly of  $\beta$ -sheets and unordered segments, similar to that described previously (Blond et al. 2002; Soudy et al. 2012). In the presence of POPC, its structure remained relatively unchanged, although some regions appeared to shift from unordered to  $\beta$ -turn in the presence of POPG or POPE. Spectra deconvoluted in order to fit conventional protein structure archetypes did not vary significantly among peptides **C1**, **7-21C**, **WK\_7-21** and MccJ25. The unordered structure of peptide **C1** decreased from 44 to 33, 34 and 32 %, in the presence of POPC, POPG or POPE, respectively. We observed that the peptide sheet conformation increased by 6 and 8 %, respectively in the presence of POPG and POPE vesicles. The  $\beta$ -sheet content of peptide **7-21C** increased from 36 to 43 % after contact with POPC. In contrast,  $\beta$ -sheet conformation decreased to 25 and 20 % in the presence of POPG or POPE vesicles, while turn structure increased by 7 %. The overall secondary structure of **WK\_7-21** remained stable in the presence of each phospholipid except for a 5–7 % decrease in unordered segments in the presence of POPG or POPE vesicles.

#### *Interaction of peptides with membrane lipids using FTIR*

Phase transitions (methylene group stretching vibration) and membrane interfacial conformation (ester group stretching vibration) of DPPG and DMPC vesicles were monitored in the absence or presence of MccJ25, **C1**, **7-21C** and **WK\_7-21** using FTIR spectroscopy.

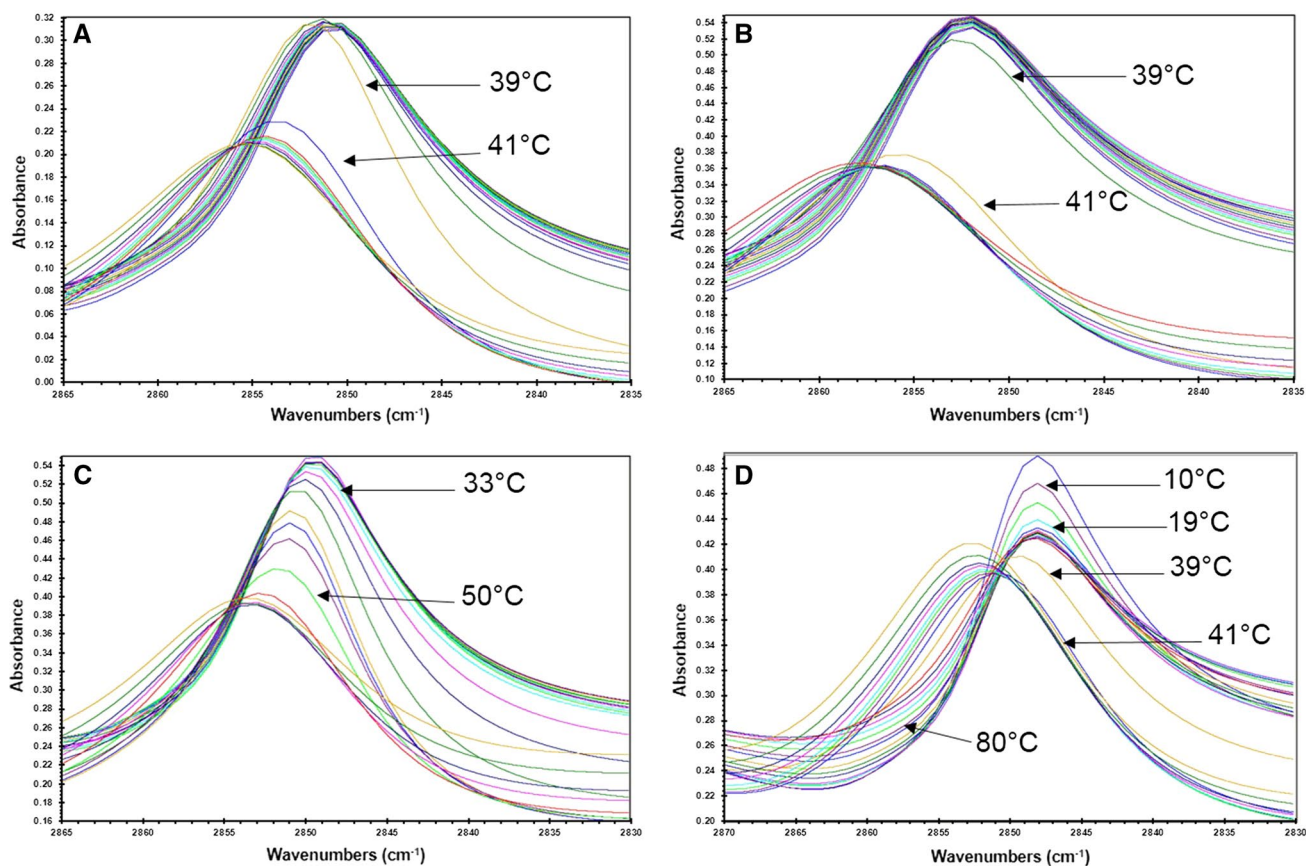
**Lipid phase transition** Two main lipid-chain C–H stretching vibration bands appear around 2,918 and 2,850  $\text{cm}^{-1}$ , assigned respectively to the anti-symmetric  $\nu_{\text{as}}(\text{CH}_2)$  and symmetric  $\nu_{\text{s}}(\text{CH}_2)$  methylene stretching modes. Thermotropism is a lipid-state transition obtained in response to changes in temperature. FTIR spectra are characterized by a shift in C–H stretching vibration bands due to lipid thermotropism. These bands have been used extensively as a probe for monitoring lipid-phase transition (Gaussier et al. 2003). Figure 7 presents the FTIR spectra of  $\text{CH}_2$  stretching vibration of DPPG as a function of temperature in the absence and presence of the different peptides.

Figure 8 shows the  $\nu_{\text{s}}(\text{CH}_2)$  thermal transition curves. The midpoint of the curves represents the transition temperatures ( $T_{\text{m}}$ ), which were 40 and 23  $^{\circ}\text{C}$ , respectively for pure DPPG and DMPC. These values are in agreement with those in the literature (Gaussier et al. 2003; Severcan and Dorohoi 2008). The mixtures of DMPC with each individual peptide all had the same  $T_{\text{m}}$  profile, indicating that none of the tested peptides interacted with or altered the conformation of the acyl chains. In contrast, the  $T_{\text{m}}$  profile obtained in the case of DPPG was different for each peptide. **C1** did not alter acyl chain conformation, since neither the  $T_{\text{m}}$  nor the wavelength of the  $\nu_{\text{s}}(\text{CH}_2)$  mode in the gel and liquid-crystalline phases were changed, while **7-21C** caused  $T_{\text{m}}$  shifts over the 33–50  $^{\circ}\text{C}$  range, indicating that it interacts with the DPPG and promotes gel phase stabilization. In the case of **WK\_7-21**, two transition stages were clearly distinguished. The first was in the 10–19  $^{\circ}\text{C}$  range, well below the transition temperature of pure DPPG, followed by a gradual transition in the 39–80  $^{\circ}\text{C}$  range. These results indicate that peptide **WK\_7-21** is able to interact with and penetrate the hydrophobic core of DPPG bilayers regardless of temperature, while peptide **7-21C** interacts with DPPG only around the transition temperature.

**Effect on membrane interfacial regions** Phospholipid-ester-group (C=O) stretching vibration appears as a band at 1,740  $\text{cm}^{-1}$ , which can provide information on the degree of hydration and conformation of the membrane interfacial region. Figure 9 shows the FTIR spectra of pure DPPG and mixtures of DPPG with each individual peptide. Like pure DPPG, the mixture of DPPG and peptide **C1** spectra showed modification at 41  $^{\circ}\text{C}$ . Around the  $T_{\text{m}}$ , the C=O stretching vibration band at 1,740  $\text{cm}^{-1}$  undergoes a sharp drop accompanied by a shift towards a longer wavenumber and a dramatic narrowing as the gel phase is converted into the liquid-crystalline phase. In the mixture of DPPG and peptide **7-21C**, this change occurred at a lower temperature range (31–37  $^{\circ}\text{C}$ ), while in the DPPG/peptide **WK\_7-21** mixture it occurred over a much wider range (10–41  $^{\circ}\text{C}$ ). No differences were observed between pure DMPC and DMPC/peptide mixtures. FTIR analysis of ester group stretching vibration confirmed the lipid-phase transition results. Peptide **WK\_7-21** is able to interact with and penetrate anionic membranes such as DPPG, while no interaction occurs in the case of zwitterionic membranes like DMPC.

#### **Discussion**

MccJ25 exhibits bactericidal activity toward several gram-negative food-borne pathogens including disease-causing pathogens such as *Salmonella* and *E. coli* (Sable et al. 2000; Vincent et al. 2004; Destoumieux-Garzón et al. 2005;



**Fig. 7** FTIR spectra showing the band corresponding to symmetric methylene stretching vibration  $\nu_s(\text{CH}_2)$  of pure DPPG at pD 6 (a) and mixtures of DPPG and peptides C1 (b), 7-21C (c) or WK\_7-21 (d)

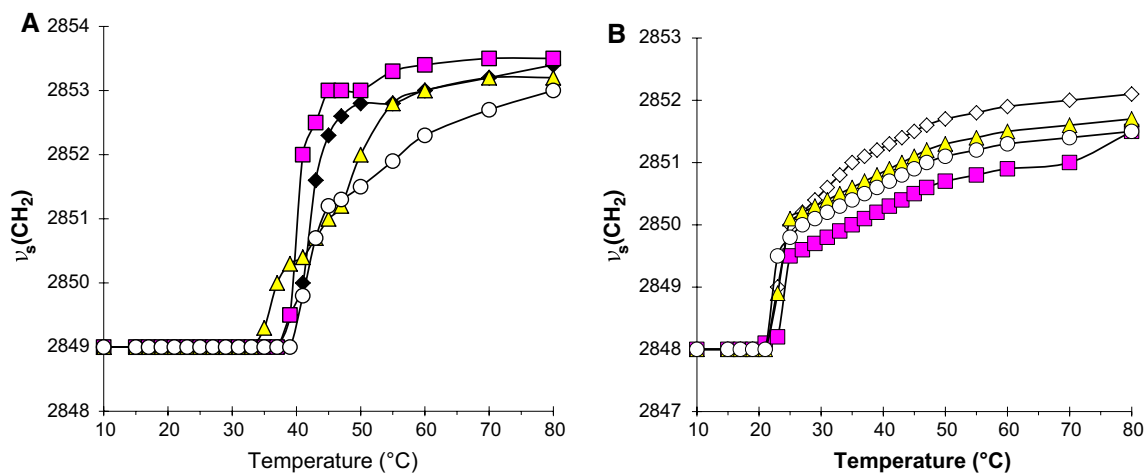


**Fig. 8** Acyl chain transition temperature for DPPG (a) and DMPC (b) in the absence or presence of the different peptides, as revealed by the shift in the  $\nu_s(\text{CH}_2)$  band of the FTIR spectra. DPPG (black

diamond); DMPC (white diamond); C1 (square); 7-21 (triangle) and WK\_7-21 (circle)

Soudy et al. 2012). The particular lasso conformation of MccJ25 makes it highly thermostable and resistant to denaturation and proteolysis, which are attractive properties for

both food and pharmaceutical applications. The structure–activity relationships of MccJ25 were previously assessed by mutational analyses and site-directed mutagenesis which

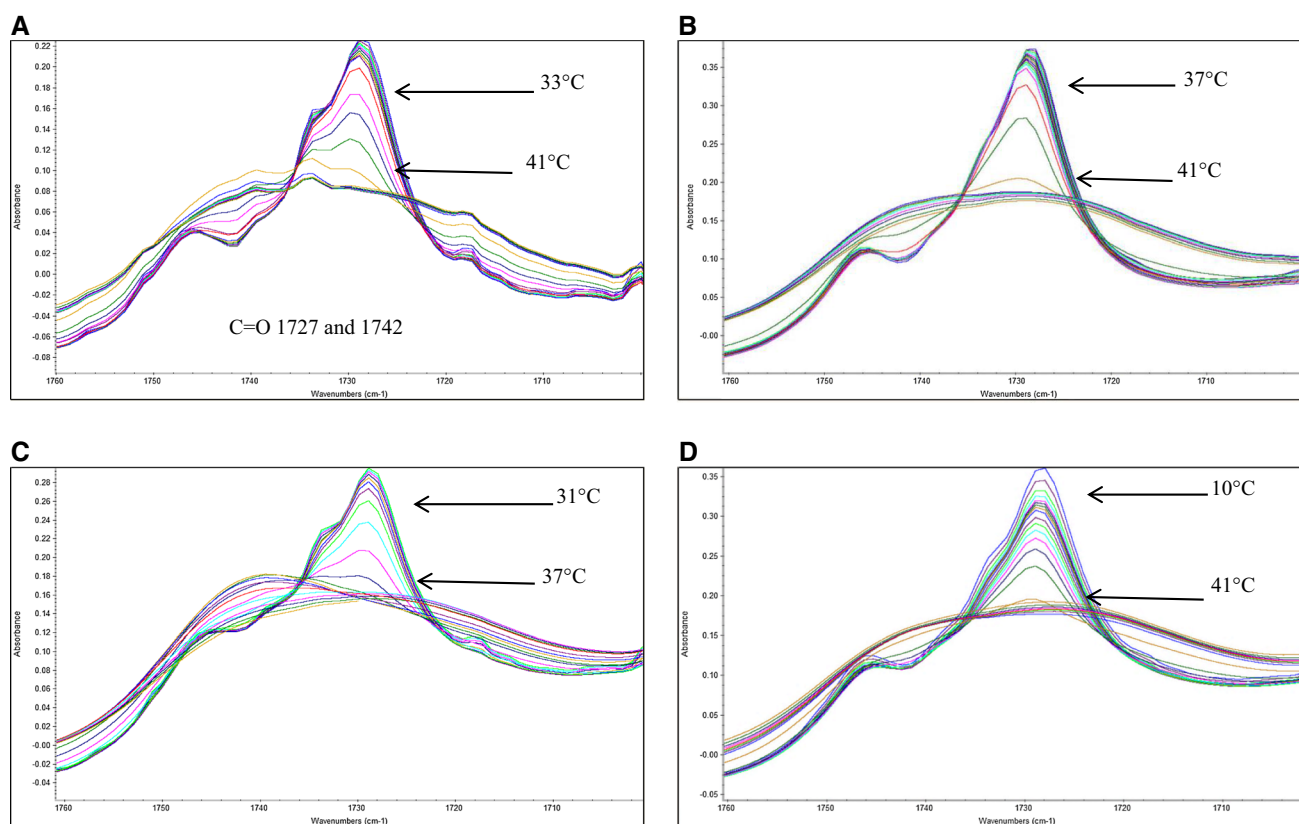


**Fig. 9** FTIR spectra showing the ester group (C=O) stretching vibration band at  $1,740\text{ cm}^{-1}$  for DPPG alone (a) and in the presence of C1 (b), 7-21C (c) and WK\_7-21 (d)

provided a more detailed information about its antibacterial activity and targets (Yuzenkova et al. 2002; Pan and Link 2011; Pavlova et al. 2008; Pan et al. 2011; Ducasse et al. 2012). These studies highlighted tolerance of MccJ25 to a number of residue substitutions.

Attempts at chemical synthesis of the lasso structure of MccJ25 so far have been unsuccessful, yielding a loop-tail topology rather than a lasso (Ferguson et al. 2010), and no synthesized derivative peptide as potent as natural MccJ25 has been reported. Based on results obtained by Soudy et al. (2012), we hypothesized that the lasso contributes to MccJ25 activity but is not essential, and that potent-derived peptides without this structure may be obtained. In this study, we synthesized various MccJ25-derived peptides, modified by substitutions and/or truncation, some of which were inhibitory to *S. enterica* and *E. coli*. Since C1, 7-21C and WK\_7-21 were all at least ten times less potent than MccJ25, the constrained lasso structure might be more than somewhat important for antibacterial action.

Soudy et al. (2012) reported antibacterial activity for similar sequences lacking lasso-folding with reduced activity compared to native microcin. Additionally, at higher concentrations, these peptides inhibited Gram-positive bacteria ( $\text{MIC} \geq 250\text{ }\mu\text{M}$ ). Peptide WK\_7-21 contains

positive charges and a hydrophobic patch, which could explain its greater interaction with membrane phospholipids. While MccJ25 uptake into bacterial cells is dependent on the FhuA receptor, WK\_7-21 could reach the cytoplasm via non-specific interactions with membrane phospholipids. A number of reports point to the potential of MccJ25 for interacting with bacterial membranes (Rintoul et al. 2001; Dupuy and Morero 2011; Dupuy et al. 2009). Dupuy et al. (2009) observed co-sedimentation of fluorescein-labeled MccJ25 with bacterial membranes, suggesting microcin-membrane interaction. In the present study, we observed based on lipid-phase transition of phospholipids that WK\_7-21 was able to interact with and penetrate anionic membranes like DPPG while no interactions occurred in the case of zwitterionic membranes such as DMPC. Increasing the number of basic and hydrophobic residues could facilitate peptide electrostatic interaction with and subsequent penetration of lipid bilayers, as has been observed for several cationic antibacterial peptides (Chan et al. 2006). This likely had an impact on the mode of action of WK\_7-21 by making it structurally similar to cationic antimicrobial peptides. Although these too interact strongly with cell membranes, they might also act on other molecular targets or cell processes by binding to a variety

of anionic and hydrophobic molecules such as DNA, proteins and cell membranes (Hale and Hancock 2007).

MccJ25 inhibits transcription by binding in the secondary channel of RNAP and thereby blocking substrate access to the catalytic site (Semenova et al. 2005). The tyrosine residue at position 9 of the MccJ25 peptide has been shown essential for RNAP inhibition with no compatible substitutions (Pavlova et al. 2008). Noteworthy, all the active peptides synthesized in this study lack the lasso structure but keep tyrosine 9, which has been shown to be essential to RNAP inhibition. Other residues, namely at positions 4 (glycine), 7 (proline), 10 (phenylalanine) and 19 (phenylalanine) are reportedly important but not strictly essential for MccJ25 binding to RNAP (Pavlova et al. 2008). In the present study, we observed that MccJ25-derived peptides lacking the lasso structure were able to inhibit *in vitro* RNAP at high concentrations (5 and 50  $\mu$ M). Although these peptides presumably bound to RNAP, it is not possible to deduce that they share a common binding site with MccJ25. Pavlova et al. (2008) reported that the RNAP/MccJ25 interaction involves primarily hydrophobic interaction. Since the active MccJ25-derived peptides had phenylalanine residues at positions 10 and 19 and tyrosine at position 9, these might be involved in the inhibition of RNAP. On the other hand, in the case of **WK\_7-21**, the KWK pattern at the N-terminus could be involved. This pattern is known to bind to DNA (Johnson et al. 1996). The respiratory apparatus of *S. enterica* could be a target for **WK\_7-21**, **C1** and **7-21C**, as it is for MccJ25. Uptake of these peptides inside cells leads to increased superoxide production, oxidative damage of biologically important molecules, and ultimately cell death. Although Soudy et al. (2012) did not report RNAP binding of the two inhibitory peptides (**1** and **6**), such activity is possible and should be investigated. Further studies are required to decipher the precise molecular mechanism of these and other MccJ25-derived peptides.

These findings put forward the possibility of producing MccJ25-derived peptides lacking the lasso structure nevertheless conserving antibacterial activity. The presence of the lasso constrains the structure of MccJ25 while conferring to it potent antibacterial activity. MccJ25-derived peptides lacking the lasso but otherwise constrained in a rigid overall structure, for example by disulfide bonds, could be strongly antibacterial. A rigid topology close to that of MccJ25 appears to make the molecule a more potent antibacterial agent. For the moment, it cannot be ruled out that the mechanisms of action of the natural MccJ25 and its synthetic derived-peptides are different.

**Acknowledgments** The authors express their gratefulness to Sophie Sablé for providing the *E. coli* strain harboring the plasmid pTUC202. François Bédard thanks the National Sciences and Engineering Research Council of Canada (NSERC) and the Fonds d'enseignement et de recherche de la Faculté de pharmacie de l'Université Laval for

scholarships. The financial support of the Fonds de recherche du Québec-Nature et technologies (FQRNT) is gratefully acknowledged.

**Conflict of interest** The authors declare that no personal relationship or interest had any influence on the design, execution, analysis or interpretation of the experiments reported herein.

## References

- Bayro MJ, Mukhopadhyay J, Swapna GVT, Huang JY, Ma L-C, Sineva E, Dawson PE, Montelione GT, Ebright RH (2003) Structure of antibacterial peptide microcin J25: a 21-residue lariat protoknot. *J Am Chem Soc* 125(41):12382–12383. doi:[10.1021/ja036677e](https://doi.org/10.1021/ja036677e)
- Bellomio A, Rintoul MR, Morero RD (2003) Chemical modification of microcin J25 with diethylpyrocarbonate and carbodiimide: evidence for essential histidyl and carboxyl residues. *Biochem Biophys Res Commun* 303(2):458–462
- Bellomio A, Vincent PA, de Arcuri BF, Salomón RA, Morero RD, Farías RN (2004) The microcin J25 beta-hairpin region is important for antibiotic uptake but not for RNA polymerase and respiration inhibition. *Biochem Biophys Res Commun* 325(4):1454–1458. doi:[10.1016/j.bbrc.2004.10.186](https://doi.org/10.1016/j.bbrc.2004.10.186)
- Bellomio A, Vincent PA, de Arcuri BF, Farías RN, Morero RD (2007) Microcin J25 has dual and independent mechanisms of action in *Escherichia coli*: RNA polymerase inhibition and increased superoxide production. *J Bacteriol* 189(11):4180–4186. doi:[10.1128/jb.00206-07](https://doi.org/10.1128/jb.00206-07)
- Blond A, Cheminant M, Destoumieux-Garzón D, Ségalas-Milazzo I, Peduzzi J, Goulard C, Rebuffat S (2002) Thermolysin-linearized microcin J25 retains the structured core of the native macrocyclic peptide and displays antimicrobial activity. *Eur J Biochem* 269(24):6212–6222
- Bollhagen R, Schmiedberger M, Barlos K, Grell E (1994) A new reagent for the cleavage of fully protected peptides synthesised on 2-chlorotriyl chloride resin. *J Chem Soc Chem Commun* 22:2559–2560. doi:[10.1039/C39940002559](https://doi.org/10.1039/C39940002559)
- Braun V (1995) Energy-coupled transport and signal transduction through the gram-negative outer membrane via TonB-ExbB-ExbD-dependent receptor proteins. *FEMS Microbiol Rev* 16(4):295–307
- Chan DI, Prenner EJ, Vogel HJ (2006) Tryptophan- and arginine-rich antimicrobial peptides: structures and mechanisms of action. *Biochim Biophys Acta* 1758(9):1184–1202. doi:[10.1016/j.bbame.2006.04.006](https://doi.org/10.1016/j.bbame.2006.04.006)
- Choudhury HG, Tong Z, Mathavan I, Li Y, Iwata S, Zirah S, Rebuffat S, van Veen HW, Beis K (2014) Structure of an antibacterial peptide ATP-binding cassette transporter in a novel outward occluded state. *Proc Natl Acad Sci USA* 111(25):9145–9150. doi:[10.1073/pnas.1320506111](https://doi.org/10.1073/pnas.1320506111)
- Clarke DJ, Campopiano DJ (2007) Maturation of McjA precursor peptide into active microcin MccJ25. *Org Biomol Chem* 5(16):2564–2566
- de Cristóbal RE, Solbiati JO, Zenoff AM, Vincent PA, Salomón RA, Yuzenkova J, Severinov K, Farías RN (2006) Microcin J25 uptake: His5 of the MccJ25 lariat ring is involved in interaction with the inner membrane MccJ25 transporter protein SbmA. *J Bacteriol* 188(9):3324–3328. doi:[10.1128/jb.188.9.3324-3328.2006](https://doi.org/10.1128/jb.188.9.3324-3328.2006)
- Delgado MA, Rintoul MR, Farías RN, Salomón RA (2001) *Escherichia coli* RNA polymerase is the target of the cyclopeptide antibiotic microcin J25. *J Bacteriol* 183(15):4543–4550. doi:[10.1128/jb.183.15.4543-4550.2001](https://doi.org/10.1128/jb.183.15.4543-4550.2001)
- Destoumieux-Garzón D, Duquesne S, Peduzzi J, Goulard C, Desmadril M, Letellier L, Rebuffat S, Boulanger P (2005) The iron-siderophore transporter FhuA is the receptor for the antimicrobial

- peptide microcin J25: role of the microcin Val11-Pro16 beta-hairpin region in the recognition mechanism. *Biochem J* 389(Pt 3):869–876. doi:[10.1042/bj20042107](https://doi.org/10.1042/bj20042107)
- Ducasse R, Yan K-P, Goulard C, Blond A, Li Y, Lescop E, Guittet E, Rebuffat S, Zirah S (2012) Sequence determinants governing the topology and biological activity of a lasso peptide, microcin J25. *ChemBioChem* 13(3):371–380. doi:[10.1002/cbic.201100702](https://doi.org/10.1002/cbic.201100702)
- Dupuy F, Morero R (2011) Microcin J25 membrane interaction: selectivity toward gel phase. *Biochim Biophys Acta* 1808(6):1764–1771. doi:[10.1016/j.bbame.2011.02.018](https://doi.org/10.1016/j.bbame.2011.02.018)
- Dupuy FG, Chirou MV, de Arcuri BF, Minahk CJ, Morero RD (2009) Proton motive force dissipation precludes interaction of microcin J25 with RNA polymerase, but enhances reactive oxygen species overproduction. *Biochim Biophys Acta* 1790(10):1307–1313. doi:[10.1016/j.bbagen.2009.07.006](https://doi.org/10.1016/j.bbagen.2009.07.006)
- Ferguson AL, Zhang S, Dikiy I, Panagiotopoulos AZ, Debenedetti PG, James Link A (2010) An experimental and computational investigation of spontaneous lasso formation in microcin J25. *Biophys J* 99(9):3056–3065. doi:[10.1016/j.bpj.2010.08.073](https://doi.org/10.1016/j.bpj.2010.08.073)
- Fields GB, Noble RL (1990) Solid-phase peptide-synthesis utilizing 9-fluorenylmethoxycarbonyl amino-acids. *Int J Pept Protein Res* 35(3):161–214
- Gaussier H, Lefèvre T, Subirade M (2003) Binding of pediocin PA-1 with anionic lipid induces model membrane destabilization. *Appl Environ Microbiol* 69(11):6777–6784. doi:[10.1128/AEM.69.11.6777-6784.2003](https://doi.org/10.1128/AEM.69.11.6777-6784.2003)
- Hale JD, Hancock RE (2007) Alternative mechanisms of action of cationic antimicrobial peptides on bacteria. *Exp Rev Anti-infect Ther* 5(6):951–959. doi:[10.1586/14787210.5.6.951](https://doi.org/10.1586/14787210.5.6.951)
- Hammami R, Zouhir A, Hamida JB, Neffati M, Vergoten G, Naghmouchi K, Fliss I (2009) Antimicrobial properties of aqueous extracts from three medicinal plants growing wild in arid regions of Tunisia. *Pharm Biol* 47(5):452–457. doi:[10.1080/13880200902822604](https://doi.org/10.1080/13880200902822604)
- Johnson NP, Mazarguil H, Lopez A (1996) Strandedness discrimination in peptide–polynucleotide complexes. *J Biol Chem* 271(33):19675–19679. doi:[10.1074/jbc.271.33.19675](https://doi.org/10.1074/jbc.271.33.19675)
- Kelly SM, Price NC (2000) The use of circular dichroism in the investigation of protein structure and function. *Curr Protein Pept Sci* 1(4):349–384
- Liu S, Zhou L, Li J, Suresh A, Verma C, Foo YH, Yap EPH, Tan DTH, Beuerman RW (2008) Linear analogues of human  $\beta$ -defensin 3: concepts for design of antimicrobial peptides with reduced cytotoxicity to mammalian cells. *ChemBioChem* 9(6):964–973. doi:[10.1002/cbic.200700560](https://doi.org/10.1002/cbic.200700560)
- Lopez FE, Vincent PA, Zenoff AM, Salomón RA, Fariás RN (2007) Efficacy of microcin J25 in biomatrices and in a mouse model of *Salmonella* infection. *J Antimicrob Chemother* 59(4):676–680. doi:[10.1093/jac/dkm009](https://doi.org/10.1093/jac/dkm009)
- Rintoul MR, de Arcuri BF, Salomón RA, Fariás RN, Morero RD (2001) The antibacterial action of microcin J25: evidence for disruption of cytoplasmic membrane energization in *Salmonella* newport. *FEMS Microbiol Lett* 204(2):265–270. doi:[10.1111/j.1574-6968.2001.tb10895.x](https://doi.org/10.1111/j.1574-6968.2001.tb10895.x)
- Mukhopadhyay J, Sineva E, Knight J, Levy RM, Ebright RH (2004) Antibacterial peptide microcin J25 inhibits transcription by binding within and obstructing the RNA polymerase secondary channel. *Mol Cell* 14(6):739–751. doi:[10.1016/j.molcel.2004.06.010](https://doi.org/10.1016/j.molcel.2004.06.010)
- Niklison Chirou M, Bellomio A, Dupuy F, Arcuri B, Minahk C, Morero R (2008) Microcin J25 induces the opening of the mitochondrial transition pore and cytochrome c release through superoxide generation. *FEBS J* 275(16):4088–4096. doi:[10.1111/j.1742-4658.2008.06550.x](https://doi.org/10.1111/j.1742-4658.2008.06550.x)
- Pan SJ, Link AJ (2011) Sequence diversity in the lasso peptide framework: discovery of functional microcin J25 variants with multiple amino acid substitutions. *J Am Chem Soc* 133(13):5016–5023. doi:[10.1021/ja1109634](https://doi.org/10.1021/ja1109634)
- Pan SJ, Cheung WL, Fung HK, Floudas CA, Link AJ (2011) Computational design of the lasso peptide antibiotic microcin J25. *Protein Eng Des Sel* 24(3):275–282. doi:[10.1093/protein/gzq108](https://doi.org/10.1093/protein/gzq108)
- Patel G, Husman W, Jehanli AM, Deadman JJ, Green D, Kakkar VV, Brennand DM (1999) A cyclic peptide analogue of the loop III region of platelet-derived growth factor-BB is a synthetic antigen for the native protein. *J Pept Res* 53(1):68–74. doi:[10.1111/j.1399-3011.1999.tb01618.x](https://doi.org/10.1111/j.1399-3011.1999.tb01618.x)
- Pavlova O, Mukhopadhyay J, Sineva E, Ebright RH, Severinov K (2008) Systematic structure–activity analysis of microcin J25. *J Biol Chem* 283(37):25589–25595. doi:[10.1074/jbc.M803995200](https://doi.org/10.1074/jbc.M803995200)
- Rosengren KJ, Clark RJ, Daly NL, Göransson U, Jones A, Craik DJ (2003) Microcin J25 has a threaded sidechain-to-backbone ring structure and not a head-to-tail cyclized backbone. *J Am Chem Soc* 125(41):12464–12474. doi:[10.1021/ja0367703](https://doi.org/10.1021/ja0367703)
- Sable S, Pons AM, Gendron-Gaillard S, Cottenceau G (2000) Antibacterial activity evaluation of microcin J25 against diarrheagenic *Escherichia coli*. *Appl Environ Microbiol* 66(10):4595–4597
- Salomón RA, Fariás RN (1993) The FhuA protein is involved in microcin 25 uptake. *J Bacteriol* 175(23):7741–7742
- Salomón RA, Fariás RN (1995) The peptide antibiotic microcin 25 is imported through the TonB pathway and the SbmA protein. *J Bacteriol* 177(11):3323–3325
- Semenova E, Yuzenkova Y, Peduzzi J, Rebuffat S, Severinov K (2005) Structure–activity analysis of microcin J25: distinct parts of the threaded lasso molecule are responsible for interaction with bacterial RNA polymerase. *J Bacteriol* 187(11):3859–3863. doi:[10.1128/jb.187.11.3859-3863.2005](https://doi.org/10.1128/jb.187.11.3859-3863.2005)
- Severcan F, Dorohoi DO (2008) FTIR studies of temperature influence on the DPPG model membrane. *J Mol Struct* 887(1–3):117–121. doi:[10.1016/j.molstruc.2008.02.039](https://doi.org/10.1016/j.molstruc.2008.02.039)
- Solbiati JO, Ciaccio M, Fariás RN, Salomón RA (1996) Genetic analysis of plasmid determinants for microcin J25 production and immunity. *J Bacteriol* 178(12):3661–3663
- Soudy R, Wang L, Kaur K (2012) Synthetic peptides derived from the sequence of a lasso peptide microcin J25 show antibacterial activity. *Bioorg Med Chem* 20(5):1794–1800. doi:[10.1016/j.bmc.2011.12.061](https://doi.org/10.1016/j.bmc.2011.12.061)
- Sreerama N, Woody RW (2004) Computation and analysis of protein circular dichroism spectra. In: Ludwig B, Michael LJ (eds) *Methods in enzymology*, vol 383. Academic Press, St Louis, pp 318–351. doi:[10.1016/S0076-6879\(04\)83013-1](https://doi.org/10.1016/S0076-6879(04)83013-1)
- Tam JP, Wu CR, Liu W, Zhang JW (1991) Disulfide bond formation in peptides by dimethyl-sulfoxide—scope and applications. *J Am Chem Soc* 113(17):6657–6662. doi:[10.1021/Ja00017a044](https://doi.org/10.1021/Ja00017a044)
- Vincent PA, Delgado MA, Fariás RN, Salomón RA (2004) Inhibition of *Salmonella enterica* serovars by microcin J25. *FEMS Microbiol Lett* 236(1):103–107. doi:[10.1016/j.femsle.2004.05.027](https://doi.org/10.1016/j.femsle.2004.05.027)
- Vincent PA, Bellomio A, de Arcuri BF, Fariás RN, Morero RD (2005) MccJ25 C-terminal is involved in RNA-polymerase inhibition but not in respiration inhibition. *Biochem Biophys Res Commun* 331(2):549–551. doi:[10.1016/j.bbrc.2005.03.220](https://doi.org/10.1016/j.bbrc.2005.03.220)
- Wilson K-A, Kalkum M, Ottesen J, Yuzenkova J, Chait BT, Landick R, Muir T, Severinov K, Darst SA (2003) Structure of microcin J25, a peptide inhibitor of bacterial RNA polymerase, is a lassoed tail. *J Am Chem Soc* 125(41):12475–12483. doi:[10.1021/ja036756q](https://doi.org/10.1021/ja036756q)
- Yan K-P, Li Y, Zirah S, Goulard C, Knappe TA, Marahiel MA, Rebuffat S (2012) Dissecting the maturation steps of the lasso peptide microcin J25 in vitro. *ChemBioChem* 13(7):1046–1052. doi:[10.1002/cbic.201200016](https://doi.org/10.1002/cbic.201200016)
- Yuzenkova J, Delgado M, Nechaev S, Savalia D, Epshtein V, Artsimovitch I, Mooney RA, Landick R, Fariás RN, Salomon R, Severinov K (2002) Mutations of bacterial RNA polymerase leading to resistance to microcin j25. *J Biol Chem* 277(52):50867–50875. doi:[10.1074/jbc.M209425200](https://doi.org/10.1074/jbc.M209425200)